PCCP

Accepted Manuscript

ROYAL SOCIETY OF CHEMISTRY

www.rsc.org/pccp

A computational mechanistic investigation of hydrogen production in water with the $[Rh^{III}(dmbpy)_2Cl_2]^+$ / $[Ru^{II}(bpy)_3]^{2+}$ / ascorbic acid photocatalytic system

Megumi Kayanuma,[a,†] Thibaut Stoll,[b] Chantal Daniel,[a] Fabrice Odobel,[c] Jérôme Fortage,[b*] Alain Deronzier,[b] Marie-Noëlle Collomb[b]*

[a] Laboratoire de Chimie Quantique, Institut de Chimie Strasbourg, UMR 7177 CNRS/UdS, 1-4 Rue Blaise Pascal, 67037 Strasbourg, France

[b] Univ. Grenoble Alpes, DCM, F-38000 Grenoble, France
CNRS, DCM, F-38000 Grenoble, France

[c] CEISAM, Université de Nantes, CNRS, Université de LUNAM, 2 rue de la Houssinière, 44322 Nantes Cedex 3, France

KEYWORDS: DFT calculation, hydrogen evolution, rhodium complex, hydride, mechanistic investigation, photocatalysis

ABSTRACT. We recently reported an efficient molecular homogeneous photocatalytic system for hydrogen (H_2) production in water combining $[Rh^{III}(dmbpy)_2Cl_2]^+$ (dmbpy = 4,4'-dimethyl-2,2'-bipyridine) as H_2 evolving catalyst, $[Ru^{II}(bpy)_3]^{2+}$ (bpy = 2,2'-bipyridine) as photosensitizer and ascorbic acid as sacrificial electron donor (*Chem. Eur. J.* **2013**, *19*, 781). Herein, the possible rhodium intermediates and mechanistic pathways for H_2 production with this system were investigated at DFT/B3LYP level of theory and the most probable reaction pathways were proposed. The calculations confirmed that the initial step of the mechanism is a reductive quenching of the excited state of the Ru photosensitizer by ascorbate, affording the reduced $[Ru^{II}(bpy)_2(bpy^{\bullet-})]^+$ form which is capable, in turn, to reduce the Rh^{III} catalyst into the distorted square planar $[Rh^{I}(dmbpy)_2]^+$ species. This two-electron reduction by $[Ru^{II}(bpy)_2(bpy^{\bullet-})]^+$ is sequential and occurs according to an ECEC mechanism which involves the release of one chloride after each one-electron reduction step of the Rh catalyst. The mechanism of disproportionation of the intermediate Rh^{II} species, much less

thermodynamically favoured, cannot be barely ruled out since it could be also favoured from a kinetic point of view. The Rh^{I} catalyst reacts with H_3O^+ to generate the hexa-coordinated hydride $[Rh^{III}(H)(dmbpy)_2(X)]^{n+}$ (X = Cl^- or H_2O), as key intermediate for H_2 release. The DFT study also revealed that the real source of proton for the hydride formation as well as the subsequent step of H_2 evolution is H_3O^+ rather than ascorbic acid, even if the latter does govern the pH of the aqueous solution. Besides, the calculations have shown that H_2 is preferentially released through an heterolytic mechanism by reaction of the $Rh^{III}(H)$ hydride and H_3O^+; the homolytic pathway, involving the reaction of two $Rh^{III}(H)$ hydrides, being clearly less favoured. In parallel to this mechanism, the reduction of the $Rh^{III}(H)$ hydride into the penta-coordinated species $[Rh^{II}(H)(dmbpy)_2]^+$ by $[Ru^{II}(bpy)_2(bpy^{\bullet-})]^+$ is also possible, according to the potentials of the respective species determined experimentally and this is confirmed by the calculations. From this $Rh^{II}(H)$ species, the heterolytic and homolytic pathways are both thermodynamically favourable to produce H_2 confirming that $Rh^{II}(H)$ is as reactive as $Rh^{III}(H)$ towards the production of H_2.

INTRODUCTION. Conversion of solar energy into electricity, thermal energy or chemical fuels has drawn much attention due to needs for clean and renewable energy source that would be an alternative to fossil fuels.[1] In this context, efficient photocatalytic production of dihydrogen (H_2) under visible-light irradiation, which is believed to be a convenient clean energy carrier for the future, is an important goal.[2-5] Most of molecular homogeneous photocatalytic systems dedicated to photo-induced H_2 production combine a photosensitizer which collects solar energy, a H_2-evolving catalyst and a sacrificial electron donor. Numerous photocatalytic systems in literature exhibit high activity in organic media or in mixtures of aqueous/organic solvents.[6-21] Those operating efficiently in fully aqueous solution were rare and limited to noble-metal based catalysts (rhodium and platinum)[22-27] until 2012, when several examples with cobalt,[28-41] iron[42-45] and nickel-based[46] catalysts were reported. Developing H_2-evolving photocatalytic systems functioning in pure water is essential for their subsequent applications in photo-electrochemical water-splitting devices.[28,47,48] Recently, we reported one of the most efficient photocatalytic system operating in purely aqueous solution which involves $[Rh^{III}(dmbpy)_2(Cl)_2]^+$ (dmbpy = 4,4'-dimethyl-2,2'-bipyridine) as H_2-evolving catalyst, $[Ru^{II}(bpy)_3]^{2+}$ (bpy = 2,2'-bipyridine) as photosensitizer, and the sodium ascorbate (HA^-)/ascorbic acid (H_2A) couple as sacrificial electron donor and protons source, respectively.[25] Under optimal conditions, at pH 4.0 with a H_2A (0.55 M)/HA^- (0.55 M) buffer, this system gave up to 1010 turnovers per catalyst molecule, with an initial turnover frequency as high as 857 h^{-1}. The performances, in terms of stability and efficiency, were further improved by chemically connecting the Rh catalyst and the Ru photosensitizer by a covalent link.[49] In both connected and unconnected systems, we have evidenced *via* transient absorption spectroscopy measurements that the initial step of the photocatalytic H_2 production is a reductive quenching of the excited state of the Ru photosensitizer by ascorbate, affording the $[Ru^{II}(bpy)_2(bpy^{\bullet-})]^+$ reduced state which is then able to reduce the Rh^{III} catalyst into $[Rh^{I}(dmbpy)_2]^+$. This Rh^I species can further react with protons to form a Rh^{III} hydride species (denoted $Rh^{III}(H)$), the key intermediate for H_2 evolution.[50] Then H_2 can evolve following different pathways: (i) $Rh^{III}(H)$ species reacts with a proton to form H_2 and the initial Rh^{III} catalyst (heterolytic route), (ii) two $Rh^{III}(H)$ species react together to generate H_2 and two Rh^{II} complexes (homolytic route) and (iii) a further reduction of $Rh^{III}(H)$ species into $Rh^{II}(H)$, which can then react *via* similar heterolytic and homolytic routes generating the Rh^{II} and Rh^I species, respectively, and H_2. Even if the first photoinduced steps of the catalytic cycle which correspond to the generation of Rh^I and then $Rh^{III}(H)$ were experimentally established,[50] the

most probable reaction pathways following the formation of $Rh^{III}(H)$ that should govern the H_2 production have not yet been evidenced. More specifically, the most favourable oxidation state of the hydride species responsible of H_2 release, $Rh^{III}(H)$ or $Rh^{II}(H)$, and the heterolytic or homolytic pathways involved in catalysis, have not been clearly identified. Many other questions are still opened, such as the nature of the coordination sphere of the various Rh intermediates as well as the real source of proton (*i.e.* ascorbic acid or H_3O^+) involved in H_2 production.

Some recent studies used successfully density functional theory (DFT) to provide mechanistic insights relative to the pathways for photoinduced hydrogen evolution catalyzed by either cobaloximes,[51-57] or a cobalt polypyridyl complex,[29] or diiron hydrogenase models[58,59], or a platinum bipyridyl complex.[60] These previous works prompt us to apply this approach to our $[Rh^{III}(dmbpy)_2Cl_2]^+/[Ru^{II}(bpy)_3]^{2+}/H_2A/HA^-$ photocatalytic system described above. We thus report herein a theoretical investigation of the mechanism of H_2 evolution with this system. For this purpose, we have analysed by DFT calculation the structural and optical properties of some of the initial complexes and of the key intermediate species. We also calculated the relative stabilities of the various intermediates responsible of the H_2 evolution, including $Rh^{III}(H)$ and $Rh^{II}(H)$ hydrides. From a thermodynamic point of view, we were able to propose the most favourable mechanistic pathways for H_2 evolution.

COMPUTATIONAL METHODS. The structures of the ruthenium and of the various rhodium complexes involved as possible intermediates in the photocatalytic system, $[Rh^{III}(dmbpy)_2(X)_2]^{n+}$, $[Rh^{III}(H)(dmbpy)_2(X)]^{n+}$ $[Rh^{III}(H)(dmbpy)_2]^{2+}$, $[Rh^{II}(dmbpy)_2(X)_2]^{n+}$ $[Rh^{II}(dmbpy)_2(X)]^{n+}$, $[Rh^{II}(H)(dmbpy)_2(X)]^{n+}$, $[Rh^{II}(H)(dmbpy)_2]^+$, $[Rh^{I}(dmbpy)_2]^+$ and $[Rh^{I}(dmbpy)_2(dmbpy^{\bullet-})]^0$ ($X = Cl^-$, H_2O, HA^-) have been optimized by means of density functional theory (DFT) with the B3LYP functional in the electronic ground state in water.[61-63] LanL2DZ (Los Alamos ECP plus DZ) basis sets have been used for ruthenium and rhodium atoms[64,65] and 6-31G(d,p) basis sets[66,67] for the others. Solvent corrections has been considered with the Polarizable Continuum Model (PCM) using the integral equation formalism variant (IEFPCM) for water ($\varepsilon = 78.3553$).[68] Vibrational analysis has been performed for all the optimized structures to confirm true energy minima and transition states. Intrinsic reaction coordinate (IRC) calculations have been carried out for each transition state to verify whether the structure connect the expected minima. A schematic picture of the thermodynamics of the reaction pathways has been obtained by free energies differences. In the present calculation, only the translational, rotational, and vibrational contributions have

been included. The solvation free energy was not considered. In order to check the effect of addition of water molecules on the system, the driving force of some reactions (entries 8, 9, 17, 18, 31 in Table 1), where H_2O participates, have been also recalculated. The comparison of the absolute $\Delta G°$ values of the two cases, in which the water molecule as reactant or product is located or not near the rhodium complex (see Table S12), show that $\Delta G°$ changes when H_2O molecules are added to the system, but the thermodynamics (exergonic or endergonic features) of each reaction is conserved and the interpretation of these driving forces is unchanged. Thus only the case, where no further H_2O molecule was added to the system, was discussed in details in this theoretical study.

The theoretical absorption spectra of $[Ru^{II}(bpy)_3]^{2+}$, $[Rh^{III}(dmbpy)_2(Cl)_2]^+$, $[Rh^{III}(dmbpy)_2(H_2O)_2]^{3+}$, $[Rh^{II}(dmbpy)_2(Cl)]^+$, $[Rh^{II}(dmbpy)_2(H_2O)]^{2+}$, $[Rh^{I}(dmbpy)_2]^+$, $[Rh^{III}(H)(dmbpy)_2(Cl)]^+$ and $[Rh^{III}(H)(dmbpy)_2(H_2O)]^{2+}$ have been calculated by means of time-dependent DFT (TD-DFT)[69,70] using Stuttgart relativistic small-core effective core potential (Stuttgart RSC 1997 ECP) with the corresponding double-ζ valence basis sets on the metal atoms[71] and Dunning double-ζ polarized (DZP) basis sets[72] for the others including solvent corrections (water). The calculations have been performed with Gaussian 09 quantum chemistry software.[73]

RESULTS AND DISCUSSION

Benchmarking of structural and optical properties. In order to validate the theoretical approach for the study of the mechanism of H_2 production, the optimized structures and the calculated absorption spectra of the ruthenium and rhodium complexes involved in H_2 evolution are commented and compared to the experimental data when available in the literature (see the supporting information for more details, Figures S1-S6 and Tables S1-S11). Among all the calculated structures, the $[Rh^{III}(dmbpy)_2(Cl)_2]^+$ and $[Rh^{I}(dmbpy)_2]^+$ complexes exhibit respectively an octahedral and distorted square-planar geometry and their optimized structure matches well with the crystallographic structure reported in literature for their analogues $[Rh^{III}(bpy)_2(Cl)_2]^+$ and $[Rh^{I}(bpy)_2]^+$.[74,75] The theoretical study also permits to define the coordination sphere of the active species for H_2 evolution, the $Rh^{III}(H)$ and $Rh^{II}(H)$ hydrides. $Rh^{III}(H)$ is a hexa-coordinated complex adopting preferentially an octahedral geometry (*i.e.* $[Rh^{III}(H)(dmbpy)_2(X)]^{n+}$, X = H_2O or Cl^-, n = 2 or 1), while $Rh^{II}(H)$ is stable in a penta-coordinated structure with a distorted square-pyramidal geometry (*i.e.* $[Rh^{II}(H)(dmbpy)_2]^+$). Although $Rh^{III}(H)$ has been isolated and characterized by spectroscopy

techniques, no structural data is available for this complex. Concerning $Rh^{II}(H)$, this species is too unstable to be observed experimentally. The UV-visible absorption spectra of all the Rh complexes were also calculated and the agreement with the experimental data was rather good (see the supporting information for more details).

Photocatalytic hydrogen production. The different possible pathways involved in H_2 evolution are shown in Figures 1-3 and their calculated free energies are listed in the Table 1.

The redox reactions in the framework of Marcus theory. The Marcus theory[76,77] correlates the kinetics of an electron transfer (k) to its driving force ($\Delta G°$) and to the global reorganization energy (λ) of the system in which the redox reaction occurs. It is well-known that, when $\Delta G° > -\lambda$, the electron transfer lies in the normal region of Marcus and its kinetics increases when the absolute value of $\Delta G°$ increases. When $\Delta G° < -\lambda$, the electron transfer is in the inverted region of Marcus and its kinetics behaves differently towards the driving force, it decreases when the absolute value of $\Delta G°$ increases. In order to determine in which region of Marcus the electron transfers are, we have calculated the reorganization energy of each electron transfer step occurring in the photocatalytic system $[Rh^{III}(dmbpy)_2Cl_2]^+/[Ru^{II}(bpy)_3]^{2+}/H_2A/HA^-$ (Entries 1-5, 28-29 in Table 1). By using the classical definition of the λ value[77] that can be expressed as sum of the inner and outer reorganization energies (see the supporting information for the calculation details, Table S13), the λ values have been estimated largely higher than 1.1 eV, which corresponds to 106.1 kJ mol^{-1}. Consequently, considering that the driving forces of electron transfers occurring in this three component system are ranging from -2.8 to -101 kJ mol^{-1} (Entries 1-5, 28-29 in Table 1), their $\Delta G°$ should be superior to $-\lambda$ and the kinetics of these processes must lie in the normal region of Marcus and should exhibit a normal behavior towards $\Delta G°$.

Table 1. Free energies (kJ mol^{-1}) of the different possible pathways involved in H_2 production.

		ΔG°
Rh^{I} formation		
1	$^3[Ru^{III}(bpy)_2(bpy^{\bullet-})]^{2+} + HA^- \rightarrow [Ru^{II}(bpy)_2(bpy^{\bullet-})]^+ + HA^\bullet$	-79.0
2	$[Rh^{III}(dmbpy)_2(Cl)_2]^+ + [Ru^{II}(bpy)_2(bpy^{\bullet-})]^+ \rightarrow [Rh^{II}(dmbpy)_2(Cl)_2] + [Ru^{II}(bpy)_3]^{2+}$	-77.2
3	$[Rh^{III}(dmbpy)_2(Cl)_2]^+ + [Ru^{II}(bpy)_2(bpy^{\bullet-})]^+ \rightarrow [Rh^{II}(dmbpy)_2(Cl)]^+ + Cl^- + [Ru^{II}(bpy)_3]^{2+}$	-98.7
4	$[Rh^{II}(dmbpy)_2(Cl)]^+ + [Ru^{II}(bpy)_2(bpy^{\bullet-})]^+ \rightarrow [Rh^{I}(dmbpy)_2]^+ + Cl^- + [Ru(bpy)_3]^{2+}$	-101.4
5	$2[Rh^{II}(dmbpy)_2(Cl)]^+ \rightarrow [Rh^{I}(dmbpy)_2]^+ + [Rh^{III}(dmbpy)_2(Cl)_2]^+$	-2.8
6	$[Rh^{I}(dmbpy)_2]^+ + [Ru^{II}(bpy)_2(bpy^{\bullet-})]^+ \rightarrow [Rh^{I}(dmbpy)(dmbpy^{\bullet-})]^0 + [Ru^{II}(bpy)_3]^{2+}$	+23.7
$Rh^{III}(H)$ hydride formation		
7	$[Rh^{I}(dmbpy)_2]^+ + H_3O^+ \rightarrow [Rh^{III}(H)(dmbpy)_2(H_2O)]^{2+}$	-102.5
8	$[Rh^{I}(dmbpy)_2]^+ + H_3O^+ \rightarrow [Rh^{III}(H)(dmbpy)_2]^{2+} + H_2O$	-95.2
9	$[Rh^{III}(H)(dmbpy)_2]^{2+} + H_2O \rightarrow [Rh^{III}(H)(dmbpy)_2(H_2O)]^{2+}$	-7.3
10	$[Rh^{III}(H)(dmbpy)_2]^{2+} + Cl^- \rightarrow [Rh^{III}(H)(dmbpy)_2(Cl)]^+$	-51.1
11	$[Rh^{III}(H)(dmbpy)_2(H_2O)]^{2+} + Cl^- \rightarrow [Rh^{III}(H)(dmbpy)_2(Cl)]^+ + H_2O$	-43.8
12	$[Rh^{III}(H)(dmbpy)_2(H_2O)]^{2+} + HA^- \rightarrow [Rh^{III}(H)(dmbpy)_2(HA)]^+ + H_2O$	-30.3
13	$[Rh^{I}(dmbpy)_2]^+ + H_2A \rightarrow [Rh^{III}(H)(dmbpy)_2]^{2+} + HA^-$	+85.6
14	$[Rh^{I}(dmbpy)_2]^+ + H_2A \rightarrow [Rh^{III}(H)(dmbpy)_2(HA)]^+$	+48.0
$Rh^{III}(H)$ reactivity towards H_2 evolution		
15	$[Rh^{III}(H)(dmbpy)_2(Cl)]^+ + H_3O^+ \rightarrow [Rh^{III}(dmbpy)_2(Cl)(H_2O)]^{2+} + H_2$	-85.9
16	$[Rh^{III}(H)(dmbpy)_2(H_2O)]^{2+} + H_3O^+ \rightarrow [Rh^{III}(dmbpy)_2(H_2O)_2]^{3+} + H_2$	-52.1
17	$[Rh^{III}(H)(dmbpy)_2(Cl)]^+ + H_3O^+ \rightarrow [Rh^{III}(dmbpy)_2(Cl)]^{2+} + H_2O + H_2$	-50.9
18	$[Rh^{III}(dmbpy)_2(Cl)]^{2+} + H_2O \rightarrow [Rh^{III}(dmbpy)_2(Cl)(H_2O)]^{2+}$	-35.0
19	$[Rh^{III}(H)(dmbpy)_2(H_2O)]^{2+} + H_3O^+ \rightarrow [Rh^{III}(dmbpy)_2(H_2O)]^{3+} + H_2O + H_2$	-11.5
20	$[Rh^{III}(dmbpy)_2(H_2O)]^{3+} + H_2O \rightarrow [Rh^{III}(dmbpy)_2(H_2O)_2]^{3+}$	-40.6
21	$[Rh^{III}(H)(dmbpy)_2(Cl)]^+ + H_2A \rightarrow [Rh^{III}(dmbpy)_2(Cl)(HA)]^+ + H_2$	+76.5
22	$[Rh^{III}(H)(dmbpy)_2(H_2O)]^{2+} + H_2A \rightarrow [Rh^{III}(dmbpy)_2(H_2O)(HA)]^{2+} + H_2$	+74.7
23	$[Rh^{III}(dmbpy)_2(Cl)]^{2+} + Cl^- \rightarrow [Rh^{III}(dmbpy)_2(Cl)_2]^+$	-84.4
24	$[Rh^{III}(dmbpy)_2(Cl)(H_2O)]^{2+} + Cl^- \rightarrow [Rh^{III}(dmbpy)_2(Cl)_2]^+ + H_2O$	-49.4
25	$[Rh^{III}(dmbpy)_2(H_2O)_2]^{3+} + 2Cl^- \rightarrow [Rh^{III}(dmbpy)_2(Cl)_2]^+ + 2H_2O$	-127.0
26	$2[Rh^{III}(H)(dmbpy)_2(H_2O)]^{2+} \rightarrow 2[Rh^{II}(dmbpy)_2(H_2O)]^{2+} + H_2$	-12.0
27	$2[Rh^{III}(H)(dmbpy)_2(Cl)]^+ \rightarrow 2[Rh^{II}(dmbpy)_2(Cl)]^+ + H_2$	+13.6
$Rh^{II}(H)$ hydride formation		
28	$[Rh^{III}(H)(dmbpy)_2(Cl)]^+ + [Ru^{II}(bpy)_2(bpy^{\bullet-})]^+ \rightarrow [Rh^{II}(H)(dmbpy)_2]^+ + Cl^- + [Ru^{II}(bpy)_3]^{2+}$	-47.8
29	$[Rh^{III}(H)(dmbpy)_2(H_2O)]^{2+} + [Ru^{II}(bpy)_2(bpy^{\bullet-})]^+ \rightarrow [Rh^{II}(H)(dmbpy)_2]^+ + H_2O + [Ru^{II}(bpy)_3]^{2+}$	-91.6
30	$[Rh^{II}(H)(dmbpy)_2]^+ + Cl^- \rightarrow [Rh^{II}(H)(dmbpy)_2(Cl)]$	+54.4
31	$[Rh^{II}(H)(dmbpy)_2]^+ + H_2O \rightarrow [Rh^{II}(H)(dmbpy)_2(H_2O)]^+$	+81.6
32	$[Rh^{III}(H)(dmbpy)_2]^{2+} + [Ru^{II}(bpy)_2(bpy^{\bullet-})]^+ \rightarrow [Rh^{II}(H)(dmbpy)_2]^+ + [Ru^{II}(bpy)_3]^{2+}$	-98.9
$Rh^{II}(H)$ reactivity towards H_2 evolution		
33	$[Rh^{II}(H)(dmbpy)_2]^+ + H_3O^+ \rightarrow [Rh^{II}(dmbpy)_2(H_2O)]^{2+} + H_2$	-155.3
34	$[Rh^{II}(dmbpy)_2(H_2O)]^{2+} + Cl^- \rightarrow [Rh^{II}(dmbpy)_2(Cl)]^+ + H_2O$	-31.0
35	$2[Rh^{II}(H)(dmbpy)_2]^+ \rightarrow 2[Rh^{I}(dmbpy)_2]^+ + H_2$	-93.7

Electron transfer reactions between $[Ru(bpy)_3]^{2+}$ and $[Rh(dmbpy)_2(Cl)_2]^+$. We previously evidenced by a transient absorption spectroscopy study[25] that the first step of the photocatalytic process is mainly a reductive quenching of the triplet excited state (^{3}MLCT) of Ru photosensitizer (denoted $[Ru^{III}(bpy)_2(bpy^{\bullet-})]^{2+}$) by the sacrificial electron donor HA^-, giving the reduced $[Ru^{II}(bpy)_2(bpy^{\bullet-})]^+$ form and the neutral radical $HA^\bullet$ (Figure 1). As an experimental proof of this mechanism, the spectral signature of $[Ru^{II}(bpy)_2(bpy^{\bullet-})]^+$ was observed in the transient absorption spectra at 510 nm in the time range between 100 ns and 200 µs.

DFT calculation confirmed that this initial reductive quenching of the excited state of Ru photosensitizer by ascorbate is thermodynamically favourable with ΔG° = -79 kJ mol^{-1} (Table 1, entry 1). Then, the potential of the reduced state $[Ru^{II}(bpy)_2(bpy^{\bullet-})]^+$ is sufficiently negative ($E_{1/2}$ = -1.50 V *vs* SCE in water[78]) to enable this species to reduce the $[Rh^{III}(dmbpy)_2(Cl)_2]^+$ catalyst into $[Rh^{I}(dmbpy)_2]^+$ (E_{pc} = -0.79 V *vs* SCE in water[25]) (Figures 2 and 3, steps 1-4).

The two-electron reduction of Rh^{III} into Rh^I was previously established by cyclic voltammetry in CH_3CN for the dmbpy derivative[25,79] through the observance of an irreversible two-electron metal-centred reduction process ($E_{pc}(Rh^{III/I})$ = -0.98 V *vs* SCE). The chemical process responsible of the irreversibility is the loss of choride ions during the reduction. At more negative potentials, the two successive reversible one-electron reductions of the bipyridyl ligands ($E_{1/2}$ = -1.47 V and -1.71 V *vs* SCE) are observed.

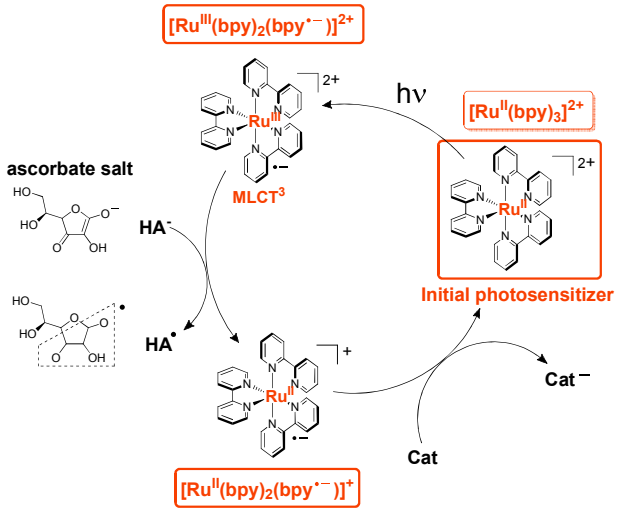

Figure 1. Reductive quenching of the Ru photosensitizer excited state by ascorbate. Cat and Cat$^-$ are respectively the ground and reduced states of the rhodium catalyst.

As previously discussed by DeArmond[79] and Meyer[80], the metal centered reduction process

could occur according to an EECC or ECEC pathway. The EECC mechanism is based on the release of two Cl^- after the two electron reductions, while the ECEC process involves the release of one chloride after each one-electron reduction step (Figures 2-3, steps 1-4). The mechanism of the two-electron reduction of Rh catalyst has never been supported by theoretical studies. DFT calculations give us a clearer insight on both mechanism aspects of the Rh catalyst reduction. From our theoretical study, it appears that the ECEC mechanism is more favourable than the EECC one, since $[Rh^{II}(dmbpy)_2(Cl)]^+ + Cl^-$ (Table 1, entries 3 and 2, respectively) is more stable by -21.5 kJ mol^{-1} than $[Rh^{II}(dmbpy)_2(Cl)_2]$ in free energy. This indicates that, after the first reduction of Rh^{III} into Rh^{II} by $[Ru^{II}(bpy)_2(bpy^{\bullet-})]^+$, the release of the first chloride ligand should be effective, affording $[Rh^{II}(dmbpy)_2(Cl)]^+$ (Figures 2-3, steps 1-2). DeArmond and coworkers[79] showed, *via* an electrochemical study in acetonitrile, that the loss of chloride ligand following the reduction $Rh^{III/II}$ is very fast.

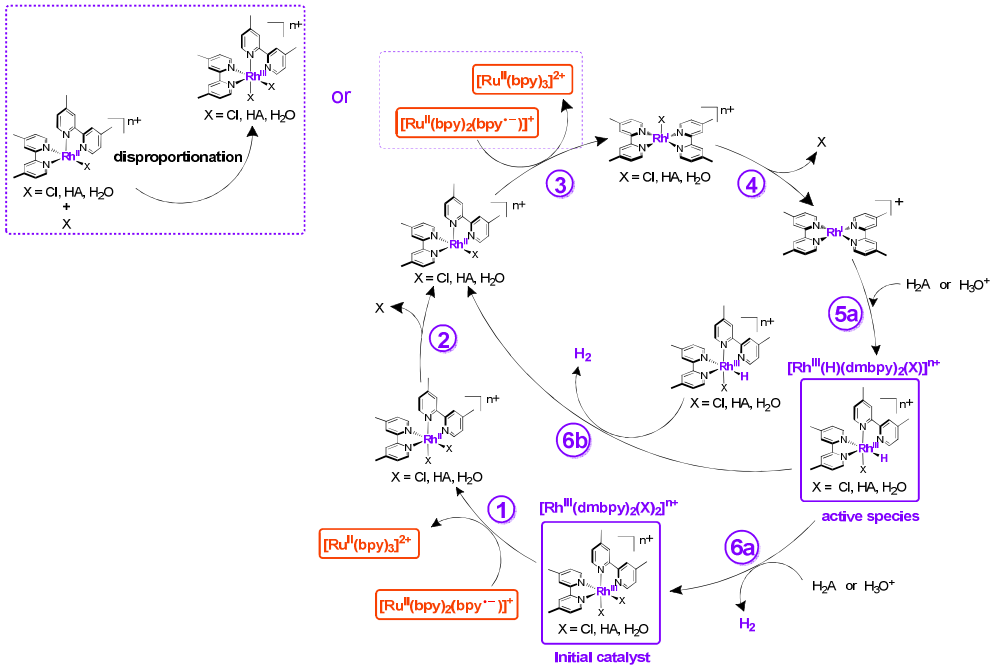

Figure 2. Possible photoinduced catalytic cycles for H_2 evolution with the $[Rh^{III}(dmbpy)_2(Cl)_2]^+/[Ru(bpy)_3]^{2+}/H_2A/HA^-$ system *via* a rhodium(III) hydride intermediate.

Then, the $[Rh^{II}(dmbpy)_2(Cl)]^+$ species should be reduced into $[Rh^{I}(dmbpy)_2(Cl)]$ by $[Ru^{II}(bpy)_2(bpy^{\bullet-})]^+$ complex. We have not obtained the theoretically calculated structure of the reduced five-coordinated species $[Rh^{I}(dmbpy)_2(Cl)]$, therefore this Rh^I complex should be unstable and could release Cl^- soon after gaining an electron from $[Ru^{II}(bpy)_2(bpy^{\bullet-})]^+$ complex, yielding the distorted square planar $[Rh^{I}(dmbpy)_2]^+$ (Table 1, entry 4). Indeed,

although the involvement of the $[Rh^{I}(dmbpy)_2(Cl)]$ species in the two-electron reduction of the rhodium catalyst was postulated in a previous study, this Rh^{I} complex was never isolated experimentally most probably due its unstable nature, which would confirm our calculations.

The disproportionation of $[Rh^{II}(dmbpy)_2(Cl)]^{+}$ which can also produce $[Rh^{I}(dmbpy)_2]^{+}$ has been considered (Table 1, entry 5) and, from a thermodynamic point of view, this process is much less favourable than the reduction by $[Ru^{II}(bpy)_2(bpy^{\bullet-})]^{+}$ (Figure 4 and Table 1, entry 4). By contrast to our photocatalytic system, Fukuzumi and co-workers[24] previously reported a similar system in which $[Rh^{III}(bpy)Cp^{*}(H_2O)]^{2+}$ (Cp^{*} = η^5-pentamethyl-cyclopentadienyl) is used as catalyst instead of $[Rh^{III}(dmbpy)_2(Cl)_2]^{+}$, and they evidenced by transient absorption spectroscopy measurements that the second step of the rhodium reduction affording Rh^{I} species occurred by disproportionation between two $[Rh^{II}(bpy)Cp^{*}(H_2O)]^{+}$. In our photocatalytic system, even though the disproportionation pathway for the second reduction of rhodium catalyst (*i.e.* $[Rh^{II}(dmbpy)_2(Cl)]^{+}$) is thermodynamically disfavoured, it could not be ruled out from the reaction mechanism since this pathway could be kinetically favoured. Further calculations on the activation barrier are needed to give a clearer answer.

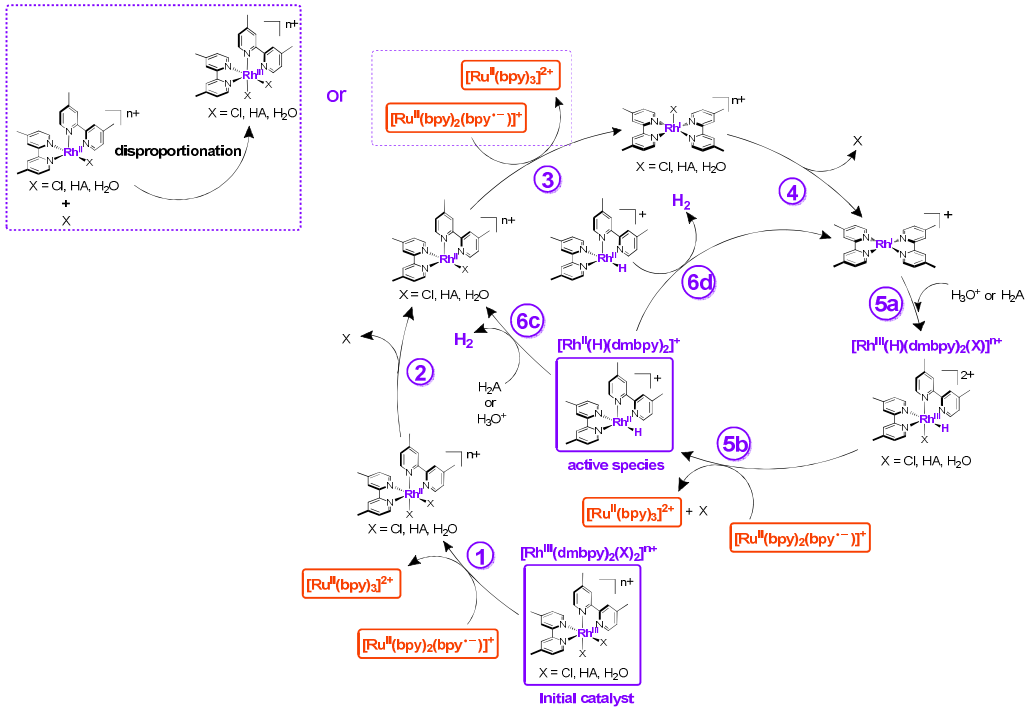

Figure 3. Possible photoinduced catalytic cycles for H_2 evolution with the $[Rh^{III}(dmbpy)_2(Cl)_2]^{+}/[Ru(bpy)_3]^{2+}/H_2A/HA^{-}$ system *via* a rhodium(II) hydride intermediate.

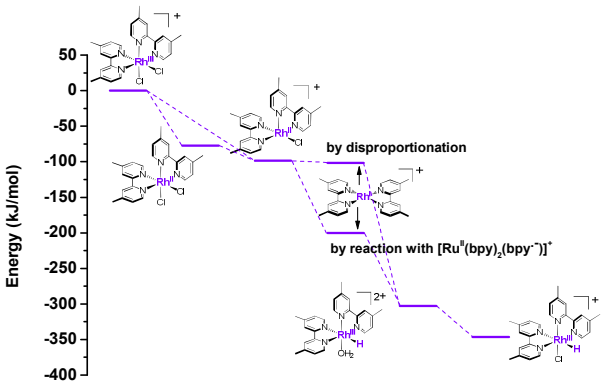

Figure 4. Calculated free energy profile for the postulated reaction pathways to form the rhodium(I) species, precursor of the rhodium(III) hydride species.

Bernhard *et al*[81] also proposed the possibility of the reduction of $[Rh^{I}(dmbpy)_2]^+$ by the reduced form of the ruthenium photosensitizer into $[Rh^{I}(dmbpy)(dmbpy^{\bullet -})]^0$, as a precursor of the Rh(H) hydride species (Table 1, entry 6). Nevertheless, this process is clearly endergonic with a driving force of +23.7 kJ mol^{-1}.

Catalytic cycle *via* $Rh^{III}(H)$ hydride species

Formation of $Rh^{III}(H)$ hydride. In this study, the hexa-coordinated Rh(III) hydride species was considered under its various potential forms: $[Rh^{III}(H)(dmbpy)_2(H_2O)]^{2+}$, $[Rh^{III}(H)(dmbpy)_2(Cl)]^+$ and $[Rh^{III}(H)(dmbpy)_2(HA)]^+$. We proposed that the formation of the $Rh^{III}(H)$ hydride (Figures 2-3, step 5a) can take place *via* two reaction pathways: the one step reaction (or concerted reaction) and the two steps reaction. In the case of the $[Rh^{III}(H)(dmbpy)_2(H_2O)]^{2+}$ hydride, the concerted reaction implies that $[Rh^{I}(dmbpy)_2]^+$ traps a proton from H_3O^+ and in the same time a molecule of H_2O coordinates to the rhodium center to generate the hexa-coordinated $[Rh^{III}(H)(dmbpy)_2(H_2O)]^{2+}$ hydride. This concerted pathway is very favourable with a driving force of -102.5 kJ mol^{-1} (Table 1, entry 7). Besides, due to the presence of the chloride and ascorbate anions in solution, the ligand exchange of H_2O in the $Rh^{III}(H)$ hydride with Cl^- or HA^- ion can also occur (Table 1, entries 11-12) and, among these ligands, Cl^- ion coordinates most strongly to the rhodium metal. Nevertheless, since water is the medium of the photocatalysis and consequently it is present in higher concentration than Cl^- ions, it could be supposed that $[Rh^{III}(H)(dmbpy)_2(H_2O)]^{2+}$ and $[Rh^{III}(H)(dmbpy)_2(Cl)]^+$ are possibly present in solution (Figure 4).

Regarding the two steps reaction for the formation of $Rh^{III}(H)$ hydride, the $[Rh^{I}(dmbpy)_2]^+$

complex gains one proton from H_3O^+ to form the $[Rh^{III}(H)(dmbpy)_2]^{2+}$ penta-coordinated hydride which is followed by the coordination of water or chloride ligand.[82] The oxidative addition of a proton to the metal occurs very easily from thermodynamic and kinetic point of view, since a high ΔG° value is obtained (-95.2 kJ mol^{-1}, Table 1, entry 8) and the potential energy curve calculated by changing Rh-H distance shows no barrier for this reaction (Figure S7). Then coordination of H_2O or Cl^- to $[Rh^{III}(H)(dmbpy)_2]^{2+}$ should occur rapidly due to the fact that the hexa-coordinated structure for the $Rh^{III}(H)$ hydride is more stable than the penta-coordinated one by 7.3 kJ mol^{-1} for $[Rh^{III}(H)(dmbpy)_2(H_2O)]^{2+}$ and by 51.1 kJ mol^{-1} for $[Rh^{III}(H)(dmbpy)_2(Cl)]^+$ (Table 1, entries 9 and 10). Actually, for this last step, two possible pathways have been considered: (i) $[Rh^{III}(H)(dmbpy)_2]^{2+}$ changes its coordination geometry with a barrier of +54.5 kJ mol^{-1} and then H_2O or Cl^- coordinates to the empty space (Figures 5a and 6a) or (ii) the coordination of H_2O or Cl^- and the change of geometry occur simultaneously with a barrier of +71.0 and +51.3 kJ mol^{-1} with H_2O and Cl^-, respectively (Figures 5b and 6b). Since the mechanism involving the structure change of rhodium complex followed by the H_2O coordination (Figure 5) has the lower activation barrier, thus it is the most favoured from a kinetic point of view. However, if a chloride ion exists near the $[Rh^{III}(H)(dmbpy)_2]^{2+}$, the second path leading to the generation of $[Rh^{III}(H)(dmbpy)_2(Cl)]^+$, where the geometry change and the Cl^- coordination take place in a concomitant manner, is slightly more favoured with a lower activation barrier (+51.3 kJ mol^{-1}) than that of the sequential one (Figure 6).

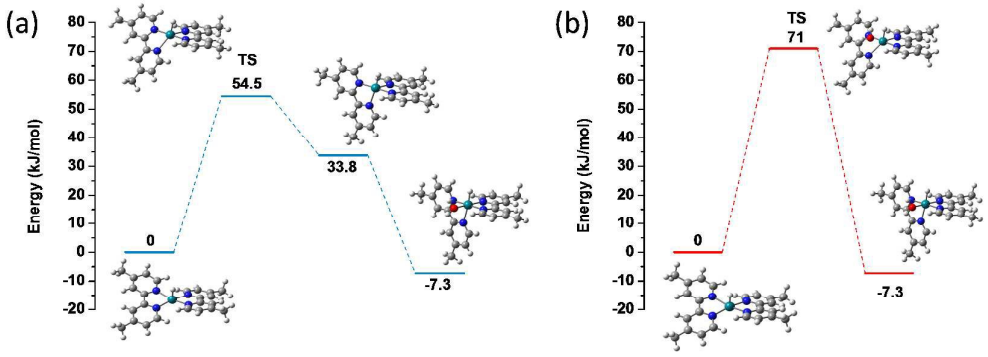

Figure 5. Calculated free energy profile for the coordination of H_2O to $[Rh^{III}(H)(dmbpy)_2]^{2+}$ complex, (a) when the change in the coordination structure is followed by H_2O coordination, or (b) when the change in the coordination structure and H_2O coordination occurs simultaneously. TS: Transition State.

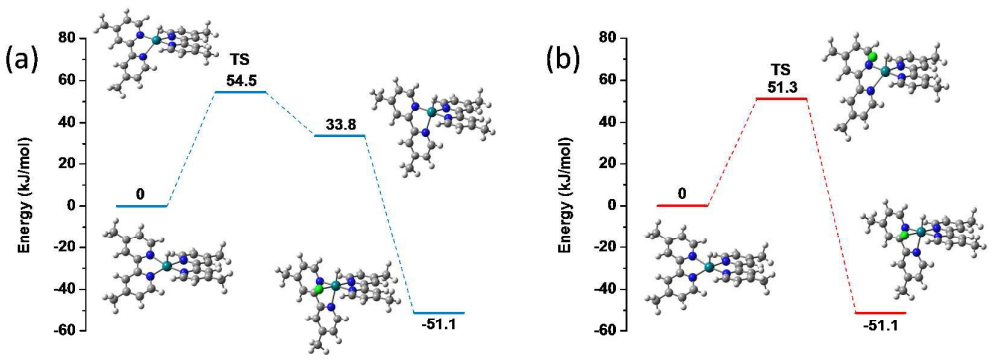

Figure 6. Calculated free energy profile for the coordination of Cl^- to $[Rh^{III}(H)(dmbpy)_2]^{2+}$ complex, (a) when the change in the coordination structure is followed by Cl^- coordination, or (b) when the change in the coordination structure and Cl^- coordination occurs simultaneously. TS: Transition State.

Comparing the concerted reaction (Table 1, entry 7) and the two steps reaction (Table 1, entries 8-10) for the formation of the $Rh^{III}(H)$ hydride species, it is difficult to discriminate which one of these both pathways is the most favourable. Nevertheless, since the rhodium(III) complex is more stable in a hexa-coordinated geometry than in a penta-coordinated geometry (*vide supra*), it could be inferred that the concerted reaction for the formation of the $Rh^{III}(H)$ hydride is the most favourable mechanism.

With the aim to obtain a more realistic system for the formation of the $Rh^{III}(H)$ hydride species, we added water molecules around the $[Rh^{I}(dmbpy)_2]^+$ complex and its co-reactant H_3O^+. Indeed, we have already observed that the surrounding water molecules reduce the proton donor ability of H_3O^+, when we have examined the effect of explicit water molecules in proton transfer reaction from H_3O^+ to $[Rh^{I}(dmbpy)_2]^+$ (Figure S7). However, this proton transfer still seems easy to occur. With three water molecules around H_3O^+, there exist a low activation barrier of 9.9 kJ mol^{-1} between the Rh^I and $Rh^{III}(H)$ species and $\{[Rh^{III}(H)(dmbpy)_2]^{2+}$ --- (H_2O) --- $3(H_2O)\}$ system is less stable than $\{[Rh^{I}(dmbpy)_2]^+$ --- (H_3O^+) --- $3(H_2O)\}$ by 7.1 kJ mol^{-1} (Figure S8). Even though the energy difference and reaction barrier between reactant and product is still small, the product will soon be stabilized by the coordination of a water molecule or a chloride ion. These calculations show that sole H_3O^+ with a PCM model is enough to evaluate the driving force of the pentacoordinated $Rh^{III}(H)$ hydride generation. We also try to investigate the effect of the addition of a water molecule on the formation of the hexacoordinated $Rh^{III}(H)$ hydride species (Table S14), since PCM model cannot incorporate the microsolvation of anion in water such as hydrogen bond

between H_2O and Cl^- or HA^-. Thus, a water molecule should stabilize the free ions compared with those coordinated to the metal. For example, we have examined the effect of a water molecule on the reaction {$[Rh^{III}(H)(dmbpy)_2]^{2+} + Cl^- \rightarrow [Rh^{III}(H)(dmbpy)_2(Cl)]^+$} (Table 1, Entry 10) in which $\Delta G°$ is -31.3 kJ mol^{-1}, while $\Delta G°$ is -51.1 kJ mol^{-1} without any additional water. For similar reaction with HA^- (*i.e.* $[Rh(dmbpy)_2(H)]^{2+} + AH^- \rightarrow [Rh(dmbpy)_2(AH)(H)]^+$, Table 1, Entries 9 + 12), $\Delta G°$ is equal to -17.5 and -37.6 kJ/mol with and without an additional water molecule. Consequently, even if the addition of water molecules decreases the $\Delta G°$ values of these reactions, they don't change the final conclusion that chloride anion coordinates most strongly to the rhodium metal and that the aqueous $Rh^{III}(H)$ derivative is the least stable hydride species.

In addition, DFT calculations allowed to highlight the source of proton at the origin of the hydride generation, by showing that $[Rh^I(dmbpy)_2]^+$ cannot gain a proton from ascorbic acid since this reaction is endergonic (Table 1, entry 13), even considering the simultaneous coordination of HA^- (Table 1, entry 14). Consequently, even if the ascorbate/ascorbic acid buffer (*i.e.* HA^-/H_2A) governs the pH of the aqueous solution, the real source of protons is most probably H_3O^+ rather than H_2A.

Reactivity of $Rh^{III}(H)$ hydride towards H_2 production. For the production of H_2, we considered two possible forms of the hexa-coordinated hydride, *i.e.* $[Rh^{III}(H)(dmbpy)_2(Cl)]^+$ and $[Rh^{III}(H)(dmbpy)_2(H_2O)]^{2+}$. From these $Rh^{III}(H)$ species, two main routes are feasible for H_2 evolution: the heterolytic and homolytic pathways (Figure 2, steps 6a and 6b).

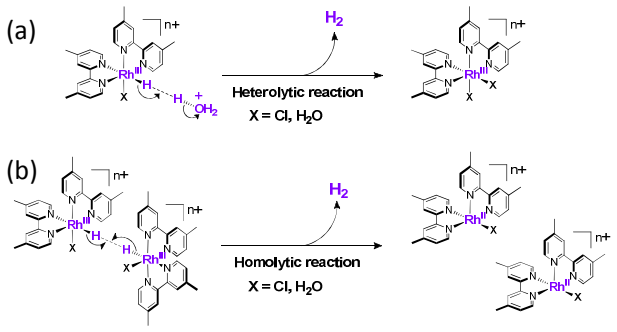

Figure 7. The heterolytic (a) and homolytic (b) pathways for H_2 production from $[Rh^{III}(H)(dmbpy)_2(X)]^{n+}$ hydride species (X = Cl^- or H_2O, n = 1 or 2).

The heterolytic path consists in a reaction between one $Rh^{III}(H)$ hydride and H_3O^+ which involves the heterolysis of the Rh-H bond and gives one molecule of H_2 and the initial $[Rh^{III}(dmbpy)_2(X)_2]^{n+}$ catalyst (X = Cl^- or H_2O; n = 1 or 3) (Figure 7a). The homolytic

mechanism is based on a reaction between two $Rh^{III}(H)$ hydrides along with a homolytic rupture of the Rh-H bond, generating one molecule of H_2 and two $[Rh^{II}(dmbpy)_2(X)]^{n+}$ (X = Cl^- or H_2O; n = 1 or 2) (Figure 7b).

Heterolytic pathway. As far as the heterolytic mechanism is concerned (Figure 2, step 6a), two reaction pathways can be envisioned: a concerted reaction and a sequential one. The concerted path suggested by Sauvage and coworkers[78] is the reaction of $Rh^{III}(H)$ hydride with H_3O^+ to evolve H_2 concomitantly to the coordination of water on the rhodium metal (Table 1, entries 15-16). From our calculations, this concerted heterolytic reaction is an exergonic process with a driving force of -85.9 and -52.1 kJ mol^{-1} from $[Rh^{III}(H)(dmbpy)_2(Cl)]^+$ and $[Rh^{III}(H)(dmbpy)_2(H_2O)]^{2+}$ respectively (Figure 8). The sequential heterolytic mechanism (or the two steps reaction), in which the hydride attack on H_3O^+ is followed by the introduction of H_2O into the coordination sphere of the rhodium metal, can be also considered (Table 1, entries 17-20). For the first step of this sequential mechanism, transition states were calculated along with a low or moderate barrier of +20.1 and +51.7 kJ mol^{-1} leading respectively to the transient metal-dihydrogen complexes, $[Rh^{III}(H_2)(dmbpy)_2(Cl)]^{2+}$ and $[Rh^{III}(H_2)(dmbpy)_2(H_2O)]^{3+}$, which are able to release rapidly H_2 and to generate the pentacoordinated $[Rh^{III}(dmbpy)_2(X)]^{n+}$ (X = Cl^- or H_2O; n = 2 or 3) (Figure 9). Similar dihydrogen intermediates were already calculated for H_2 evolution with various cobaloximes as catalyst.[55,56]

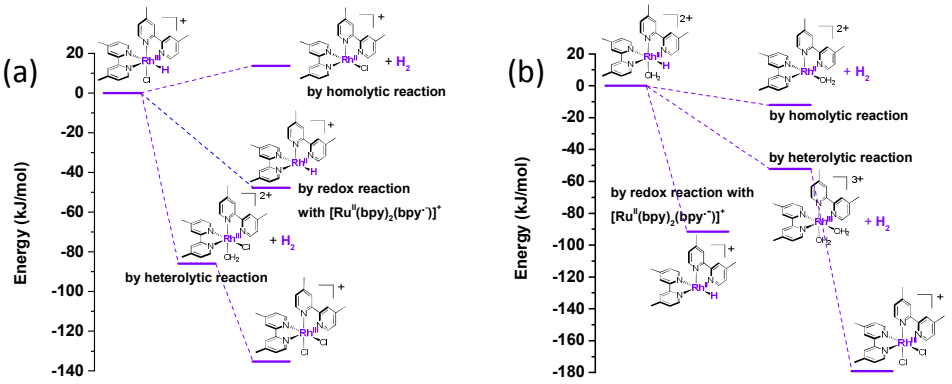

Figure 8. Calculated free energy profile for the production of H_2 from the hydride species (a) $[Rh^{III}(H)(dmbpy)_2(Cl)]^+$, (b) $[Rh^{III}(H)(dmbpy)_2(H_2O)]^{2+}$.

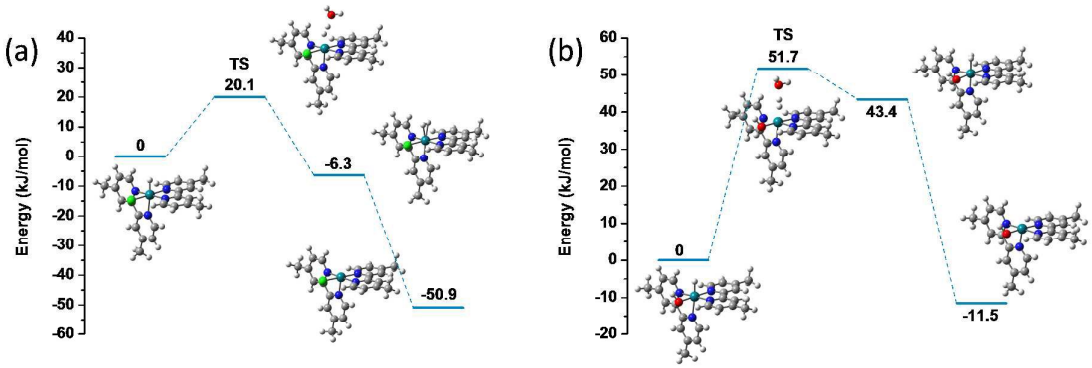

Figure 9. Calculated free energy profile for the production of H_2 through the first step of the sequential heterolytic reaction *via* the intermediates $[Rh^{III}(H_2)(dmbpy)_2(Cl)]^{2+}$ (a) and $[Rh^{III}(H_2)(dmbpy)_2(H_2O)]^{3+}$ (b). TS: Transition States.

The first step of the sequential mechanism (Table 1, entries 17 and 19) is globally exergonic with a driving force of -50.9 and -11.5 kJ mol^{-1} from $[Rh^{III}(H)(dmbpy)_2(Cl)]^{+}$ and $[Rh^{III}(H)(dmbpy)_2(H_2O)]^{2+}$ respectively. Then, sequential or simultaneous coordination of H_2O molecule stabilize the 5-coordinated product by 35.0 and 40.6 kJ mol^{-1} for $[Rh^{III}(dmbpy)_2(Cl)]^{2+}$ and $[Rh^{III}(dmbpy)_2(H_2O)]^{3+}$ respectively (Figure 9, Table 1, entries 18-20). Ascorbic acid was also considered as a possible source of the second proton required for H_2 evolution, but the reaction between the $Rh^{III}(H)$ hydride and H_2A turned out to be disfavoured from a thermodynamic point of view (Table 1, entries 21-22). This confirms that the main source of proton for H_2 evolution most probably stems from the H_3O^+ ion.

In fine, the heterolytic reaction between $[Rh^{III}(H)(dmbpy)_2(X)]^{n+}$ hydride (x = H_2O or Cl, respectively n = 2 or 1) and H_3O^+ regenerates the initial Rh^{III} catalyst which can display several possible forms (*i.e.* $[Rh^{III}(dmbpy)_2(H_2O)_2]^{3+}$, $[Rh^{III}(dmbpy)_2(Cl)(H_2O)]^{2+}$, $[Rh^{III}(dmbpy)_2(Cl)_2]^{+}$), since two different ligands can be coordinated to the rhodium metal (Cl^- and H_2O). Coordination of Cl^- anion to $[Rh^{III}(dmbpy)_2(Cl)]^{2+}$ (Table 1, entry 23) or ligand exchange within $[Rh^{III}(dmbpy)_2(Cl)(H_2O)]^{2+}$ (Table 1, entry 24) or $[Rh^{III}(dmbpy)_2(H_2O)_2]^{3+}$ (Table 1, entry 25), generating in all cases the original catalyst $[Rh^{III}(dmbpy)_2(Cl)_2]^{+}$, are exergonic reactions with a driving force of -84.4, -49.4 and -127.0 kJ mol^{-1}, respectively. It is interesting to note that, among the three possible forms of the Rh^{III} species, the chloride derivative (*i.e.* $[Rh^{III}(dmbpy)_2(Cl)_2]^{+}$) is the most stable complex.

Homolytic pathway. The H_2 production from two $[Rh^{III}(H)(dmbpy)_2(H_2O)]^{2+}$ hydride *via* a homolytic pathway was also envisaged (Table 1, entry 28 and Figure 2, step 6b), but it is less

favourable from a thermodynamic point of view (ΔG° = -12.0 kJ mol^{-1}) compared to the heterolytic pathway with H_3O^+ (Table 1, entry 16, ΔG° = -52.1 kJ mol^{-1}). If two $[Rh^{III}(H)(dmbpy)_2(Cl)]^+$ hydrides react together, the H_2 generation is clearly disfavoured with a driving force of +13.6 kJ mol^{-1} (Table 1, entry 27). Despite the fact that the heterolytic mechanism seems more probable from a thermodynamic point of view for both forms of $Rh^{III}(H)$ hydride species, both homolytic and heterolytic reaction pathways could be potentially involved in the process of H_2 production since their kinetics have not been determined and could be close (Figure 8).

Catalytic cycle *via* $Rh^{II}(H)$ hydride species

Formation of $Rh^{II}(H)$ hydride. In parallel of heterolytic and homolytic pathways from $Rh^{III}(H)$ hydride, another route can be considered which is the reduction of $Rh^{III}(H)$ into $Rh^{II}(H)$ (Figure 3, step 5b). This reaction pathway was proposed first in the eighties by Mulazzani and co-workers[83,84] and more recently by Bernhard and co-workers.[81] Very recently, we succeeded to generate the $[Rh^{III}(H)(dmbpy)_2(Cl)]^+$ hydride in CH_3CN by electrochemical reduction of the $[Rh^{III}(dmbpy)_2(Cl)_2]^+$ complex in presence of formic acid and a reduction potential value of E_{pc} = -1.34 V *vs* SCE for the couple $Rh^{III}(H)/Rh^{II}(H)$ has been determined.[50] According to this value, the reduced state of the ruthenium photosensitizer, $[Ru^{II}(bpy)_2(bpy^{\bullet-})]^+$ ($E_{1/2}$ = -1.50 V vs SCE[78]), should be able to reduce the $Rh^{III}(H)$ into $Rh^{II}(H)$. Calculations show that this reduction is actually exergonic (ΔG° = -47.8 and -91.6 kJ mol^{-1} from $[Rh^{III}(H)(dmbpy)_2(Cl)]^+$ and $[Rh^{III}(H)(dmbpy)_2(H_2O)]^{2+}$, respectively) (Table 1, entries 28-29) and the resulting product is a penta-coordinated $[Rh^{II}(H)(dmbpy)_2]^+$ hydride (Figure 8 and S4). In fact, by contrast to the $Rh^{III}(H)$ hydride (*vide supra*), the penta-coordinated structure is more stable than the hexa-coordinated structure for the $Rh^{II}(H)$ hydride. This tendency to adopt a penta-coordinated geometry is confirmed by the fact that coordination of Cl^- or H_2O to $[Rh^{II}(H)(dmbpy)_2]^+$ is not favourable (Table 1, entries 30-31). Examples of $Rh^{II}(H)$ hydride are scarce but, for instance, Savéant and co-workers[85] reported a penta-coordinated geometry for a $Rh^{II}(H)$ porphyrin hydride. Another reaction pathway for the formation of $[Rh^{II}(H)(dmbpy)_2]^+$ hydride, resulting from the reduction of the penta-coordinated $[Rh^{III}(H)(dmbpy)_2]^{2+}$ hydride, was envisaged (Table 1, entry 32). Even if the latter species is a hypothetical intermediate (*vide supra*), its reduction is clearly exergonic with a driving force of -98.9 kJ mol^{-1} when the change of coordination structure is considered (Table 1, entry 32) and of -64.3 kJ mol^{-1} when $[Rh^{II}(H)(dmbpy)_2]^+$ has already a structure similar to that of $[Rh^{III}(H)(dmbpy)_2]^{2+}$. DFT calculations also show that the reduction of

$[Rh^{III}(H)(dmbpy)_2(Cl)]^+$ (Table 1, entry 28) is less favourable than its reaction with H_3O^+ to produce H_2 molecule (heterolytic pathway) (Table 1, entry 15), while the reduction of $[Rh^{III}(H)(dmbpy)_2(H_2O)]^{2+}$ (Table 1, entry 29) has a stronger driving force than its reaction with H_3O^+ for H_2 evolution (Figure 8 and Table 1, entry 16). Because we did not evaluate the activation barriers of each reaction (i.e. the reduction of the $Rh^{III}(H)$ hydride species and its reaction with H_3O^+), it is not possible to discriminate these processes, but it could be suggested that both $Rh^{III}(H)$ and $Rh^{II}(H)$ hydrides should be involved in H_2 production.

Reactivity of $Rh^{II}(H)$ hydride towards H_2 production. Similarly to the $Rh^{III}(H)$ hydride species, the H_2 evolution from $[Rh^{II}(H)(dmbpy)_2]^+$ can take place *via* two competitive reaction pathways: heterolytic and homolytic routes (Figure 3, steps 6c and 6d and Figure 10). The heterolytic pathway, which consists of a reaction between $[Rh^{II}(H)(dmbpy)_2]^+$ and H_3O^+, producing one H_2 molecule and the Rh^{II} species, is a very exergonic reaction (ΔG° = -155.3 kJ mol^{-1}, Table 1, entry 33). During this reaction, coordination of H_2O to the rhodium center might occur. Then exchange of H_2O ligand along with chloride anion can take place (Table 1, entry 34), regenerating the intermediate $[Rh^{II}(dmbpy)_2(Cl)]^+$, initially formed by reduction of $[Rh^{III}(dmbpy)_2(Cl)_2]^+$ by $[Ru^{II}(bpy)_2(bpy^{\bullet-})]^+$ (Table 1, entry 3). Interestingly, the homolytic route leading to H_2 production from two $[Rh^{II}(H)(dmbpy)_2]^+$ (Table 1, entry 35) is also very favourable in terms of thermodynamics (ΔG° = -93.7 kJ mol^{-1}) though less favourable than the heterolytic path (Table 1, entry 35). From a general point of view, these calculations confirm that $Rh^{II}(H)$ hydride is as reactive as $Rh^{III}(H)$ hydride towards protons or itself, allowing a highly efficient catalysis of H_2 evolution.

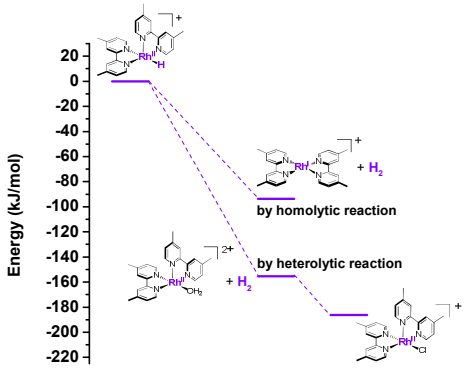

Figure 10. Calculated free energy profile for the production of H_2 from the $[Rh^{II}(H)(dmbpy)_2]^+$ hydride species.

Most probable pathways for the photocatalytic system. Figure 11 summarizes the most probable reaction pathways stemming from the DFT calculations for the photocatalytic

$[Rh^{III}(dmbpy)_2(Cl)_2]^+/[Ru(bpy)_3]^{2+}/H_2A/HA^-$ system which involve both rhodium(III) and a rhodium(II) hydride intermediates. The theoretical study confirmed that the initial step of the photocatalytic cycle is the reductive quenching of the Ru photosensitizer excited state by ascorbate, affording $[Ru^{II}(bpy)_2(bpy^{\bullet-})]^+$. The next step is the reduction of the Rh^{III} catalyst following an ECEC mechanism: the one-electron reduction of $[Rh^{III}(dmbpy)_2(Cl)_2]^+$ by $[Ru^{II}(bpy)_2(bpy^{\bullet-})]^+$ induces the very fast release of one choride to form the pentacoordinated $[Rh^{II}(dmbpy)_2(Cl)]^+$ species, which is, in turn reduced by $[Ru^{II}(bpy)_2(bpy^{\bullet-})]^+$ inducing the fast release of the second choride to give the distorted square-planar $[Rh^{I}(dmbpy)_2]^+$ (Figure 11, steps 1-4). The disproportionation of the intermediate $[Rh^{II}(dmbpy)_2(Cl)]^+$ species, much more thermodynamically disfavourable compared to its reduction through $[Ru^{II}(bpy)_2(bpy^{\bullet-})]^+$, cannot be barely ruled out since it could be also favoured from a kinetic point of view. Then, $[Rh^{I}(dmbpy)_2]^+$ complex gains one proton from H_3O^+ and coordinates H_2O or Cl^- ligand *via* a sequential or a concerted pathway to give the active species for H_2 evolution, *i.e.* the hexacoordinated $[Rh^{III}(H)(dmbpy)_2(H_2O)]^{2+}$ and $[Rh^{III}(H)(dmbpy)_2(Cl)]^+$ hydride species (Figure 11, step 5a). DFT study also revealed that the real source of proton for the hydride formation is H_3O^+ rather than H_2A, even if the couple HA^-/H_2A does govern the pH of the aqueous solution.

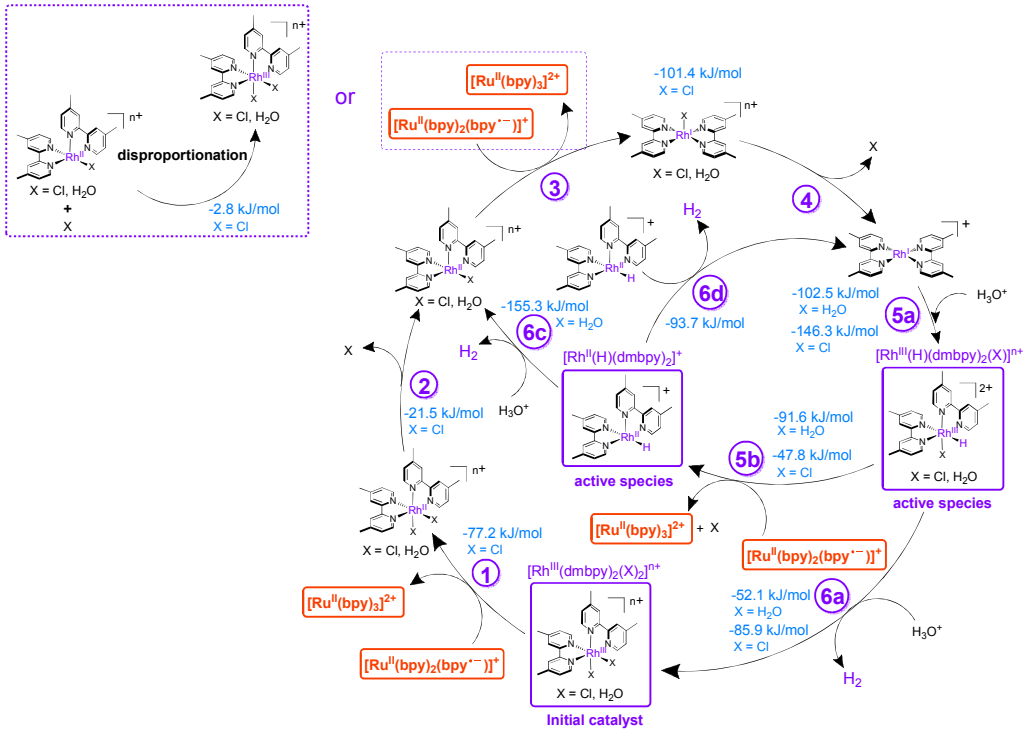

Figure 11. Most favourable pathways for H_2 evolution with the $[Rh^{III}(dmbpy)_2(Cl)_2]^+/[Ru(bpy)_3]^{2+}/H_2A/HA^-$ photocatalytic system in water.

From the $Rh^{III}(H)$ hydride, H_2 evolution can occurs following two possible pathways. One of these is the heterolytic path between $Rh^{III}(H)$ and H_3O^+, regenerating the initial $[Rh^{III}(dmbpy)_2(X)_2]^{n+}$ catalyst (X = Cl^- or H_2O) (Figure 11, step 6a); the homolytic pathway by reaction of two $Rh^{III}(H)$ leading to $[Rh^{II}(dmbpy)_2(X)]^{n+}$ (X = Cl^- or H_2O) being clearly less favoured (Figure 2, step 6b). The other favourable path for H_2 production is the reduction of $Rh^{III}(H)$ into $[Rh^{II}(H)(dmbpy)_2]^+$ by $[Ru^{II}(bpy)_2(bpy^{\bullet-})]^+$ (Figure 11, step 5b). From this species, both heterolytic (reaction with H_3O^+) and homolytic (reaction of two $Rh^{II}(H)$) routes are very favourable pathways to evolve H_2 (Figure 11, steps 6c and 6d). In spite of the lack of examples in the literature of $Rh^{II}(H)$ hydride, theoretical study suggests that it is penta-coordinated (*i.e.* $[Rh^{II}(H)(dmbpy)_2]^+$), contrary to the $Rh^{III}(H)$ hydride which is hexa-coordinated. Besides, the study showed that the reduction of $Rh^{III}(H)$ to $Rh^{II}(H)$ is also thermodynamically possible. From these results, it appears that H_2 evolution can follow different reaction pathways that could proceed in parallel *via* hetero/homolytic processes from both $Rh^{III}(H)$ and $Rh^{II}(H)$ species. The high efficiency for H_2 production in water of the photocatalytic system $[Ru^{II}(bpy)_3]^{2+}/[Rh^{III}(dmbpy)_2(Cl)_2]^+/H_2A/HA^-$ could thus be ascribed to the high reactivity of the $Rh^{III}(H)$ hydride species *vis-à-vis* protons, but also to that of $Rh^{II}(H)$.

CONCLUSION. The mechanism of photocatalytic hydrogen production by the molecular $[Rh^{III}(dmbpy)_2(Cl)_2]^+/[Ru^{II}(bpy)_3]^{2+}$/ascorbic acid system in aqueous solution has been analysed by DFT calculations. This study has provided mechanistic insight that cannot be obtained experimentally and has permitted to propose the most thermodynamically favourable mechanistic pathways for H_2 evolution that proceeds through both $Rh^{III}(H)$ and $Rh^{II}(H)$ hydride species, the key intermediates for catalytic hydrogen release. From $Rh^{III}(H)$ species, the calculations have shown that H_2 is preferentially released through an heterolytic mechanism since the homolytic pathway is less favoured. In contrast, both hetero- and homolytic mechanisms are thermodynamically favourable to evolve H_2 from the $Rh^{II}(H)$ species. Calculations clearly indicate that $Rh^{II}(H)$ is as reactive as $Rh^{III}(H)$ towards the production of H_2. Consequently the involvement of both $Rh^{III}(H)$ and $Rh^{II}(H)$ hydride species in the mechanism of H_2 production could explain the high efficiency of the photocatalytic system. Otherwise the theoretical study allowed to establish the coordination sphere of the $Rh^{III}(H)$ and $Rh^{II}(H)$ hydride. The $Rh^{III}(H)$ hydride adopts preferentially a hexa-coordinated octahedral geometry while the $Rh^{II}(H)$ hydride is penta-coordinated complex and displays a distorted square-pyramidal geometry. DFT study also revealed that the real source of proton for the hydride formation and the H_2 release is H_3O^+ rather than H_2A, even if the couple

HA^-/H_2A does govern the pH of the aqueous solution. This theoretical study has permitted to explore the possible reaction pathways, but it did not enable to discriminate the different paths and to indicate which one of them dominates in the H_2 evolution mechanism. Basically, the thermodynamic feature of each catalytic step has been calculated in this study while the kinetic aspect, which depends on the concentration of all species present in solution and the efficiency of each reaction pathway, was not fully studied and has to be further investigated. The investigation of both thermodynamic and kinetic features of reaction pathways is essential for the elucidation of the mechanism and for rational design of more effective catalysts for H_2 production in fully aqueous solution.

Electronic supplementary information (ESI) available: Optimized structures and UV-Visible absorption spectra in water of ruthenium photosensitizer and various rhodium complexes. A detailed discussion of theoretical data and a comparison with experimental data available in the literature are also given.

AUTHOR INFORMATION

Corresponding Authors

kayanuma.megumi.fw@u.tsukuba.ac.jp; jerome.fortage@ujf-grenoble.fr

Present addresses

†Graduate School of Systems and Information Engineering, University of Tsukuba, Tennodai 1-1-1, Tsukuba 305-8573, Japan

ACKNOWLEDGEMENTS

The authors thank the Agence Nationale de Recherche (ANR) through the ANR Blanc "HeteroCop" (ANR-09-BLAN-0183-01) and the ANR Blanc "PhotoBioMet" (ANR-09-BLAN-0191-01) and the LABEX ARCANE (ANR-11-LABX-0003-01) (project H_2Photocat) for financial support. The quantum chemical calculations have been performed thanks to the computer facilities of the High Performance Computing regional centre of Unistra and on the computer nodes of the LCQS, Strasbourg. The COST action CM1202 PERSPECT-H2O is also acknowledged.

REFERENCES

(1) Armaroli, N.; Balzani, V. *Angew. Chem., Int. Ed. Engl.* **2007**, *46*, 52.

(2) Esswein, M. J.; Nocera, D. G. *Chem. Rev.* **2007**, *107*, 4022.

(3) McDaniel, N. D.; Bernhard, S. *Dalton Trans.* **2010**, *39*, 10021.

(4) Teets, T. S.; Nocera, D. G. *Chem. Commun.* **2011**, *47*, 9268.

(5) Armaroli, N.; Balzani, V. *ChemSusChem* **2011**, *4*, 21.

(6) Rau, S.; Walther, D.; Vos, J. G. *Dalton Trans.* **2007**, 915.

(7) Sakai, K.; Ozawa, H. *Coord. Chem. Rev.* **2007**, *251*, 2753.

(8) Wang, M.; Na, Y.; Gorlov, M.; Sun, L. C. *Dalton Trans.* **2009**, 6458.

(9) Tinker, L. L.; McDaniel, N. D.; Bernhard, S. *J. Mater. Chem.* **2009**, *19*, 3328.

(10) Losse, S.; Vos, J. G.; Rau, S. *Coord. Chem. Rev.* **2010**, *254*, 2492.

(11) Artero, V.; Chavarot-Kerlidou, M.; Fontecave, M. *Angew. Chem. Int. Ed.* **2011**, *50*, 7238.

(12) Wang, M.; Chen, L.; Li, X.; Sun, L. *Dalton Trans.* **2011**, *40*, 12793.

(13) Du, P.; Eisenberg, R. *Energy Environ. Sci.* **2012**, *5*, 6012.

(14) Eckenhoff, W. T.; Eisenberg, R. *Dalton Trans.* **2012**, *41*, 13004.

(15) Schulz, M.; Karnahl, M.; Schwalbe, M.; Vos, J. G. *Coord. Chem. Rev.* **2012**, *256*, 1682.

(16) Manbeck, G. F.; Brewer, K. J. *Coord. Chem. Rev.* **2013**, *257*, 1660.

(17) Halpin, Y.; Pryce, M. T.; Rau, S.; Dini, D.; Vos, J. G. *Dalton Trans.* **2013**, *42*, 16243.

(18) Frischmann, P. D.; Mahata, K.; Würthner, F. *Chem. Soc. Rev.* **2013**, *42*, 1847.

(19) Wang, N.; Wang, M.; Chen, L.; Sun, L. *Dalton Trans.* **2013**, *42*, 12059.

(20) Han, Z.; Eisenberg, R. *Acc. Chem. Res.* **2014**, *47*, 2537.

(21) Berardi, S.; Drouet, S.; Francas, L.; Gimbert-Surinach, C.; Guttentag, M.; Richmond, C.; Stoll, T.; Llobet, A. *Chem. Soc. Rev.* **2014**.

(22) Oishi, S. *J. Mol. Catal.* **1987**, *39*, 225.

(23) Bauer, R.; Werner, H. A. F. *Int. J. Hydrogen Energy* **1994**, *19*, 497.

(24) Fukuzumi, S.; Kobayashi, T.; Suenobu, T. *Angew. Chem. Int. Ed.* **2011**, *50*, 728.

(25) Stoll, T.; Gennari, M.; Serrano, I.; Fortage, J.; Chauvin, J.; Odobel, F.; Rebarz, M.; Poizat, O.; Sliwa, M.; Deronzier, A.; Collomb, M. N. *Chem. Eur. J.* **2013**, *19*, 782.

(26) Ozawa, H.; Yokoyama, Y.; Haga, M.-a.; Sakai, K. *Dalton Trans.* **2007**, 1197.

(27) Stoll, T.; Castillo, C. E.; Kayanuma, M.; Daniel, C.; Odobel, F.; Fortage, J.; Collomb, M.-N. *Coord. Chem. Rev* **2015**, DOI:10.1016/j.ccr.2015.02.002.

(28) Guttentag, M.; Rodenberg, A.; Kopelent, R.; Probst, B.; Buchwalder, C.; Brandstätter, M.; Hamm, P.; Alberto, R. *Eur. J. Inorg. Chem.* **2012**, 59.

(29) Singh, W. M.; Baine, T.; Kudo, S.; Tian, S.; Ma, X. A. N.; Zhou, H.; DeYonker, N. J.; Pham, T. C.; Bollinger, J. C.; Baker, D. L.; Yan, B.; Webster, C. E.; Zhao, X. *Angew. Chem. Int. Ed.* **2012**, *51*, 5941.

(30) Guttentag, M.; Rodenberg, A.; Bachmann, C.; Senn, A.; Hamm, P.; Alberto, R. *Dalton Trans.* **2013**, *42*, 334.

(31) Bachmann, C.; Guttentag, M.; Spingler, B.; Alberto, R. *Inorg. Chem.* **2013**, *52*, 6055.

(32) Varma, S.; Castillo, C. E.; Stoll, T.; Fortage, J.; Blackman, A. G.; Molton, F.;

Deronzier, A.; Collomb, M.-N. *PhysChemChemPhys* **2013**, *15*, 17544.

(33) Singh, W. M.; Mirmohades, M.; Jane, R. T.; White, T. A.; Hammarström, L.; Thapper, A.; Lomoth, R.; Ott, S. *Chem. Commun.* **2013**, *49*, 8638.

(34) Sun, Y. J.; Sun, J. W.; Long, J. R.; Yang, P. D.; Chang, C. J. *Chem. Sci.* **2013**, *4*, 118.

(35) Nippe, M.; Khnayzer, R. S.; Panetier, J. A.; Zee, D. Z.; Olaiya, B. S.; Head-Gordon, M.; Chang, C. J.; Castellano, F. N.; Long, J. R. *Chem. Sci.* **2013**, *4*, 3934.

(36) Khnayzer, R. S.; Thoi, V. S.; Nippe, M.; King, A. E.; Jurss, J. W.; El Roz, K. A.; Long, J. R.; Chang, C. J.; Castellano, F. N. *Energy & Environmental Science* **2014**, *7*, 1477.

(37) Tong, L.; Zong, R.; Thummel, R. P. *J. Am. Chem. Soc.* **2014**, *136*, 4881.

(38) Bachmann, C.; Probst, B.; Guttentag, M.; Alberto, R. *Chem. Commun.* **2014**, *50*, 6737.

(39) Natali, M.; Luisa, A.; lengo, E.; Scandola, F. *Chem. Commun.* **2014**, *50*, 1842.

(40) Deponti, E.; Luisa, A.; Natali, M.; Iengo, E.; Scandola, F. *Dalton Trans.* **2014**, *43*, 16345.

(41) Vennampalli, M.; Liang, G.; Katta, L.; Webster, C. E.; Zhao, X. *Inorg. Chem.* **2014**, *53*, 10094.

(42) Cao, W. N.; Wang, F.; Wang, H. Y.; Chen, B.; Feng, K.; Tung, C. H.; Wu, L. Z. *Chem. Commun.* **2012**, *48*, 8081.

(43) Li, X. Q.; Wang, M.; Zheng, D. H.; Han, K.; Dong, J. F.; Sun, L. C. *Energy Environ. Sci.* **2012**, *5*, 8220.

(44) Lakadamyali, F.; Kato, M.; Muresan, N. M.; Reisner, E. *Angew. Chem. Int. Ed.* **2012**, *51*, 9381.

(45) Orain, C.; Quentel, F.; Gloaguen, F. *ChemSusChem* **2014**, *7*, 638.

(46) Weingarten, A. S.; Kazantsev, R. V.; Palmer, L. C.; McClendon, M.; Koltonow, A. R.; SamuelAmanda, P. S.; Kiebala, D. J.; Wasielewski, M. R.; Stupp, S. I. *Nat Chem* **2014**, *advance online publication*.

(47) Probst, B.; Guttentag, M.; Rodenberg, A.; Hamm, P.; Alberto, R. *Inorg. Chem.* **2011**, *50*, 3404.

(48) Stubbert, B. D.; Peters, J. C.; Gray, H. B. *J. Am. Chem. Soc.* **2011**, *133*, 18070.

(49) Stoll, T.; Gennari, M.; Fortage, J.; Castillo, C. E.; Rebarz, M.; Sliwa, M.; Poizat, O.; Odobel, F.; Deronzier, A.; Collomb, M.-N. *Angew. Chem. Int. Ed.* **2014**, *53*, 1654.

(50) Castillo, C. E.; Stoll, T.; Fortage, J.; Kayanuma, M.; Daniel, C.; Odobel, F.; Deronzier, A.; Collomb, M.-N. *submitted*.

(51) Solis, B. H.; Hammes-Schiffer, S. *Inorg. Chem.* **2011**, *50*, 11252.

(52) Solis, B. H.; Hammes-Schiffer, S. *J. Am. Chem. Soc.* **2011**, *133*, 19036.

(53) Muckerman, J. T.; Fujita, E. *Chem. Commun.* **2011**, *47*, 12456.

(54) Bhattacharjee, A.; Chavarot-Kerlidou, M.; Andreiadis, E. S.; Fontecave, M.; Field, M. J.; Artero, V. *Inorg. Chem.* **2012**, *51*, 7087.

(55) Jiang, Y.-K.; Liu, J.-H. *Int. J. Quantum Chem.* **2012**, *112*, 2541.

(56) Bhattacharjee, A.; Andreiadis, E. S.; Chavarot-Kerlidou, M.; Fontecave, M.; Field, M. J.; Artero, V. *Chem. Eur. J.* **2013**, *19*, 15166.

(57) Solis, B. H.; Yu, Y.; Hammes-Schiffer, S. *Inorg. Chem.* **2013**, *52*, 6994.

(58) Wright, R. J.; Zhang, W.; Yang, X.; Fasulo, M.; Tilley, T. D. *Dalton Trans.* **2012**, *41*, 73.

(59) Liu, Y.-C.; Chu, K.-T.; Jhang, R.-L.; Lee, G.-H.; Chiang, M.-H. *Chem. Commun.* **2013**, *49*, 4743.

(60) Ogawa, M.; Ajayakumar, G.; Masaoka, S.; Kraatz, H.-B.; Sakai, K. *Chemistry – A European Journal* **2011**, *17*, 1148.

(61) Becke, A. D. *J. Chem. Phys.* **1993**, *98*, 5648.

(62) Lee, C. T.; Yang, W. T.; Parr, R. G. *Phys. Rev. B* **1988**, *37*, 785.

(63) Stephens, P. J.; Devlin, F. J.; Chabalowski, C. F.; Frisch, M. J. *J. Phys. Chem.* **1994**, *98*, 11623.

(64) Hay, P. J.; Wadt, W. R. *J. Chem. Phys.* **1985**, *82*, 270.

(65) Hay, P. J.; Wadt, W. R. *J. Chem. Phys.* **1985**, *82*, 299.

(66) Hehre, W. J.; Ditchfield, R.; Pople, J. A. *J. Chem. Phys.* **1972**, *56*, 2257.

(67) Francl, M. M.; Pietro, W. J.; Hehre, W. J.; Binkley, J. S.; Gordon, M. S.; Defrees, D. J.; Pople, J. A. *J. Chem. Phys.* **1982**, *77*, 3654.

(68) Tomasi, J.; Mennucci, B.; Cammi, R. *Chem. Rev.* **2005**, *105*, 2999.

(69) Bauernschmitt, R.; Ahlrichs, R. *Chem. Phys. Lett.* **1996**, *256*, 454.

(70) Marques, M. A. L.; Gross, E. K. U. *Annu. Rev. Phys. Chem.* **2004**, *55*, 427.

(71) Andrae, D.; Haussermann, U.; Dolg, M.; Stoll, H.; Preuss, H. *Theor Chim. Acta* **1990**, *77*, 123.

(72) Dunning Jr., T. H.; Hay, P. J. *In Methods of Electronic Structure Theory, Plenum Press, New York* **1977**, *3*, 1.

(73) Frisch, M. J.; Trucks, G. W.; Schlegel, H. B.; Scuseria, G. E.; Robb, M. A.; Cheeseman, J. R.; Scalmani, G.; Barone, V.; Mennucci, B.; Petersson, G. A.; Nakatsuji, H.; Caricato, M.; Li, X.; Hratchian, H. P.; Izmaylov, A. F.; Bloino, J.; Zheng, G.; Sonnenberg, J. L.; Hada, M.; Ehara, M.; Toyota, K.; Fukuda, R.; Hasegawa, J.; Ishida, M.; Nakajima, T.; Honda, Y.; Kitao, O.; Nakai, H.; Vreven, T.; Montgomery, J. A., Jr.; Peralta, J. E.; Ogliaro, F.; Bearpark, M.; Heyd, J. J.; Brothers, E.; Kudin, K. N.; Staroverov, V. N.; Keith, T.; Kobayashi, R.; Normand, J.; Raghavachari, K.; Rendell, A.; Burant, J. C.; Iyengar, S. S.; Tomasi, J.; Cossi, M.; Rega, N.; Millam, J. M.; Klene, M.; Knox, J. E.; Cross, J. B.; Bakken, V.; Adamo, C.; Jaramillo, J.; Gomperts, R.; Stratmann, R. E.; Yazyev, O.; Austin, A. J.; Cammi, R.; Pomelli, C.; Ochterski, J. W.; Martin, R. L.; Morokuma, K.; Zakrzewski, V. G.; Voth, G. A.; Salvador, P.; Dannenberg, J. J.; Dapprich, S.; Daniels, A. D.; Farkas, O.; Foresman, J. B.; Ortiz, J. V.; Cioslowski, J.; Fox, D. J. *Gaussian 09, Revision B.01; , Gaussian, Inc.: Wallingford, CT, 2010*.

(74) Dikhtiarenko, A.; Laura Torre-Fernandez, L.; Garcia-Granda, S.; Garcıa, J. R.;

Gimeno, J. *Acta Cryst.* **2012**, *E68*, m713.

(75) Fujita, E.; Brunschwig, B. S.; Creutz, C.; Muckerman, J. T.; Sutin, N.; Szalda, D.; van Eldik, R. *Inorg. Chem.* **2006**, *45*, 1595.

(76) Marcus, R. A. *Annu. Rev. Phys. Chem.* **1964**, *15*, 155.

(77) Marcus, R. A.; Sutin, N. *Biochim. Biophys. Acta* **1985**, *811*, 265.

(78) Kirch, M.; Lehn, J. M.; Sauvage, J. P. *Helv. Chim. Acta* **1979**, *62*, 1345.

(79) Kew, G.; DeArmond, K.; Hanck, K. *J. Phys. Chem.* **1974**, *78*, 727.

(80) Bolinger, C. M.; Story, N.; Sullivan, B. P.; Meyer, T. J. *Inorg. Chem.* **1988**, *27*, 4582.

(81) Cline, E. D.; Adamson, S. E.; Bernhard, S. *Inorg. Chem.* **2008**, *47*, 10378.

(82) Ascorbate ion was not considered in the two steps reaction, since chloride ion is a better coordinating ligand and water is present in solution in higher concentration.

(83) Mulazzani, Q. G.; Emmi, S.; Hoffman, M. Z.; Venturi, M. *J. Am. Chem. Soc.* **1981**, *103*, 3362.

(84) Mulazzani, Q. G.; Venturi, M.; Hoffman, M. Z. *J. Phys. Chem.* **1982**, *86*, 242.

(85) Grass, V.; Lexa, D.; Savéant, J.-M. *J. Am. Chem. Soc.* **1997**, *119*, 7526.

TABLE OF CONTENT

The involvement of the $Rh^{III}(H)$ and $Rh^{II}(H)$ hydride species in the mechanism of H_2 production could explain the high efficiency of the photocatalytic system.